Magnetism and superconductivity in a heavy-fermion superconductor, $CePt_3Si$

2004 J. Phys.: Condens. Matter 16 L333

(http://iopscience.iop.org/0953-8984/16/28/L03)

INSTITUTE OF PHYSICS PUBLISHING JOURNAL OF PHYSICS: CONDENSED MATTER

J. Phys.: Condens. Matter **16** (2004) L333–L342 PII: S0953-8984(04)81248-7

LETTER TO THE EDITOR

Magnetism and superconductivity in a heavy-fermion superconductor, $CePt_3Si$

T Takeuchi[1,5], S Hashimoto[2], T Yasuda[2], H Shishido[2], T Ueda[2], M Yamada[2], Y Obiraki[2], M Shiimoto[2], H Kohara[2], T Yamamoto[2], K Sugiyama[1,2], K Kindo[1], T D Matsuda[3], Y Haga[3], Y Aoki[4], H Sato[4], R Settai[2] and Y Ōnuki[2,3]

[1] Research Centre for Materials Science at Extreme Conditions, Osaka University, Toyonaka, Osaka 560-8513, Japan
[2] Graduate School of Science, Osaka University, Toyonaka, Osaka 560-0043, Japan
[3] Advanced Science Research Centre, Japan Atomic Energy Research Institute, Tokai, Ibaraki 319-1195, Japan
[4] Department of Physics, Tokyo Metropolitan University, Minami-Ohsawa 1-1, Hachioji, Tokyo 192-0397, Japan

E-mail: takeuchi@rcem.osaka-u.ac.jp

Received 26 May 2004
Published 2 July 2004
Online at stacks.iop.org/JPhysCM/16/L333
doi:10.1088/0953-8984/16/28/L03

Abstract

We have studied the magnetic and thermal properties of a single crystal of $CePt_3Si$, which is a recently reported heavy-fermion superconductor with a superconducting transition temperature $T_c = 0.75$ K and a Néel temperature $T_N = 2.2$ K. The overall experimental data are principally explained on the basis of the crystalline electric field (CEF) scheme. Even in the antiferromagnetic state, the CEF model applies well to the characteristic features in the magnetization curve. These results indicate the existence of a localized magnetic moment at the Ce site, with a considerably reduced ordered moment of 0.16 μ_B/Ce, and the strongly correlated conduction electrons are condensed into the superconducting state. We have also constructed the magnetic phase diagram including the superconducting phase for $H \parallel [110]$ and [001].

Recently, Bauer *et al* [1] reported heavy-fermion superconductivity and antiferromagnetic ordering in $CePt_3Si$ with the tetragonal crystal structure (space group $P4mm$). A characteristic feature of this compound is a lack of inversion symmetry in the crystal structure, that is the absence of the mirror plane along the c-axis ([001] direction). This compound exhibits antiferromagnetic order at $T_N = 2.2$ K and is condensed into a heavy-fermion superconducting state at $T_c = 0.75$ K. A large Sommerfeld constant $\gamma = 350$ mJ K^{-2} mol^{-1},

[5] Address for correspondence: Low Temperature Centre, Osaka University, Toyonaka, Osaka 560-0043, Japan.

together with a large A (=2.35 $\mu\Omega$ cm K^{-2}) value in the electrical resistivity $\rho = \rho_0 + AT^2$, indicates a Fermi liquid state with significant renormalization due to electron correlations. Moreover, a large slope of the upper critical field H_{c2} at T_c, $dH_{c2}/dT = -8.5$ T K^{-1}, and a large value of $H_{c2}(0) = 5$ T indicate heavy quasiparticles forming Cooper pairs. $CePt_3Si$ is thus characterized as the first superconductor among the cerium compounds where superconductivity is realized in the long-range antiferromagnetic state, because superconductivity in the prototype heavy-fermion superconductor $CeCu_2Si_2$ [3] and the quasi-two-dimensional superconductor $CeCoIn_5$ [4] occurs in the non-magnetic or antiferromagnetically spin-fluctuating state. Phenomenologically, the superconductivity in $CePt_3Si$ is similar to that in the antiferromagnetic, superconducting uranium compounds such as UPd_2Al_3 with $T_N = 14$ K and $T_c = 1.8$ K [5].

Quite recently, Metoki *et al* [2] performed neutron scattering experiments on $CePt_3Si$. They observed the antiferromagnetic Bragg reflections with $q = (00\frac{1}{2})$. The magnetic moments of 4f electrons lie ferromagnetically in the c-plane, and are stacked antiferromagnetically along the c-axis. The magnitude of the ordered moment is considerably reduced to 0.16 μ_B/Ce. Two inelastic peaks were also observed at 1 and 24 meV. They attributed these peaks to the crystalline electric field (CEF) excitations of the localized 4f electrons from the ground state to the first and second excited states, respectively.

In this letter, we present the experimental results on a single crystal of $CePt_3Si$ obtained by measuring the electrical resistivity, specific heat, magnetic susceptibility, high-field magnetization, thermal expansion and magnetostriction. The experimental results are discussed on the basis of the CEF model. Moreover, we have constructed the magnetic and superconducting phase diagram.

Polycrystal samples were synthesized by arc-melting under an argon atmosphere using 99.9% (3N) pure Ce, 4N Pt and 5N Si in the stoichiometric proportion. These polycrystals were inserted in a molybdenum crucible, which was heated up to 1450 °C and cooled down to room temperature. That is, single crystals were grown by both the Bridgman method and mineralization. The direction of the crystal structure was determined by the x-ray Laue pattern, and a sample with the size of $2 \times 2 \times 1.5$ mm^3 was prepared for the thermal expansion measurement, for example.

The temperature dependence of the electrical resistivity ρ for the current $J \parallel [100]$ and [001] is shown in figure 1(a). Qualitatively, the behaviour is almost the same for [100] and [001]. The resistivity shows two shoulder-like features around 70 and 6 K, which are caused by the interplay between the CEF and Kondo effects. Upon further decreasing the temperature, the resistivity shows a small anomaly at $T_N = 2.3$ K, starts to drop precipitously at about 0.80 K and becomes zero at $T_c = 0.64$ K, as shown in the inset of figure 1(a). These features are in good agreement with the previous results on a polycrystal sample [1]. Here, we note that the residual resistivity ρ_0 and the residual resistivity ratio RRR ($=\rho_{RT}/\rho_0$) for $J \parallel [001]$ were $\rho_0 = 0.9$ $\mu\Omega$ cm and RRR = 106, respectively, which are compared to $\rho_0 = 5$ $\mu\Omega$ cm and RRR = 18 in the polycrystal sample in [1].

The antiferromagnetic and superconducting phase transitions were also confirmed by the present specific heat measurement, as shown in figure 1(b). The specific heat exhibits a clear λ-shape peak at T_N, but the anomaly associated with the superconducting transition at T_c is weak. In order to determine the ideal values at the two transitions, we carried out a simple equal entropy construction by a linear extrapolation of the experimental data at temperatures higher and lower than the transition temperature, as shown by thin solid lines in figure 1(b). The transition temperatures are thus determined as $T_c = 0.51$ K and $T_N = 2.3$ K, respectively. The superconducting transition temperature is slightly lower than that determined from the resistivity measurement.

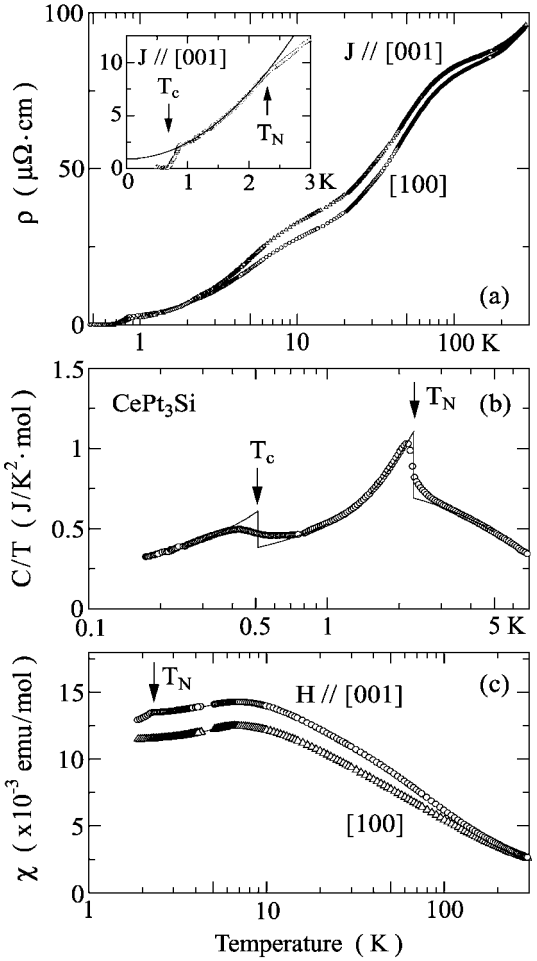

Figure 1. Temperature dependences of the electrical resistivity with the current $J \parallel [100]$ and [001] (a), specific heat in the form of C/T (b) and magnetic susceptibility for $H \parallel [001]$ and [100] (c) in $CePt_3Si$. The solid curve in the inset of (a) is the fitting curve with the form of $\rho = \rho_0 + AT^2$, where $\rho_0 = 0.9\ \mu\Omega$ cm and $A = 1.56\ \mu\Omega$ cm K^{-2}, in the temperature range from 1 K to $T_N = 2.3$ K. The solid lines in (b) represent ideal transitions determined from an equal entropy construction.

The temperature dependence of the magnetic susceptibility χ shows a broad peak around 7 K for both directions, as shown in figure 1(c). This might be due to a combined phenomenon of the CEF effect and a moment reduction due to the Kondo effect. The susceptibility for $H \parallel [001]$ shows a kink at $T_N = 2.3$ K and decreases with decreasing temperature, whereas the susceptibility for $H \parallel [100]$ only shows a continuous mild decrease across T_N. In a simple two-sublattice antiferromagnet, the parallel susceptibility $\chi_\parallel$, where the magnetic field is applied parallel to the sublattice moments, decreases below T_N and becomes zero at $T = 0$ K, while the perpendicular susceptibility $\chi_\perp$ is constant below T_N. As mentioned above, the ordered moments lie in the c-plane ((001) plane) [2]. Therefore, the observed magnetic susceptibility below T_N cannot be understood on the basis of the simple sublattice model. This problem might be related to a small localized moment.

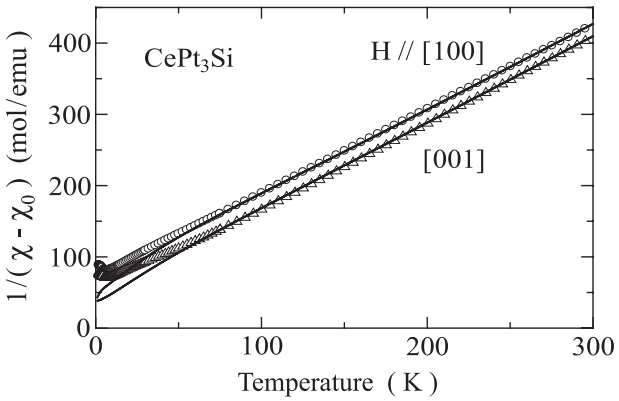

Figure 2. The temperature dependence of the inverse magnetic susceptibility in $CePt_3Si$. Solid lines are the calculated curves based on the CEF model.

The susceptibility follows the Curie–Weiss law above 100 K, but the estimated effective moment is somewhat larger than the theoretical value of 2.54 μ_B/Ce for Ce^{3+}: $\mu_{eff} = 2.75\ \mu_B$/Ce and $\Theta_p = -74.8$ K for $H \parallel [100]$ and $\mu_{eff} = 2.67\ \mu_B$/Ce and $\Theta_p = -44.9$ K for $H \parallel [001]$. In figure 2 we plotted the experimental results on the susceptibility in the form of $1/(\chi - \chi_0)$, where χ_0 was determined as 1.9×10^{-4} and 1.4×10^{-4} emu mol^{-1} for $H \parallel [100]$ and [001], respectively, so an effective magnetic moment of 2.54 μ_B/Ce is obtained above 100 K. These values of χ_0 are only 5% and 7% of the magnitude of the susceptibility at 300 K for respective directions. Two solid lines in figure 2 indicate the results of the CEF calculation, which is described later.

The experimental high-field magnetization curves M for $H \parallel [100]$ and [001] at 1.3 and 4.2 K are shown in figure 3(a). The magnetization for $H \parallel [100]$ at 1.3 K indicates a weak metamagnetic-like increase around 25 T and reaches a saturation value of about 1 μ_B/Ce at higher fields. Even at 4.2 K, which is above $T_N = 2.3$ K, the metamagnetic-like behaviour is still visible around 20 T. On the other hand, the magnetization for $H \parallel [001]$ at 1.3 K increases gradually in low fields and shows a kink at 25 T. The kink around 25 T becomes weak and broad at 4.2 K, but can still be recognized as a bend in the magnetization. The magnitude of the magnetization reaches about 0.8 μ_B/Ce at 50 T, with is five times as large as the ordered moment of 0.16 μ_B determined by the neutron scattering experiment [2]. The present characteristic features in the magnetization at 4.2 K for both field directions clearly indicate that this is not due to the antiferromagnetic ordering.

The magnetization anomaly in the paramagnetic state is observed in the heavy-fermion compounds such as $CeRu_2Si_2$ [6] and UPt_3 [7]. The metamagnetic transition in these compounds is observed as a steep increase of the magnetization at H_m, which is linearly related to the characteristic temperature $T_{\chi_{max}}$ where the magnetic susceptibility becomes maximum [8]: $H_m = 8$ T and $T_{\chi_{max}} = 8$ K in $CeRu_2Si_2$, and 20 T and 18 K in UPt_3. Here, a value of $H_m = 25$ T in $CePt_3Si$ is appreciably larger than a value expected from $T_{\chi_{max}} = 7$ K. The present magnetization anomaly is thus different from the metamagnetic transition observed in some heavy-fermion compounds. We will explain it on the basis of the level crossing effect in the 4f CEF levels as shown in figure 3(b), which will be discussed later.

We show in figure 4 the temperature dependence of the magnetic specific heat C_{mag} ($=C(CePt_3Si) - C(LaPt_3Si)$) and the thermal expansion coefficient α, which is defined by $\alpha = d(\Delta\ell/\ell)/dT$, along [110] and [001]. Above $T_N = 2.3$ K, C_{mag} exhibits a broad peak

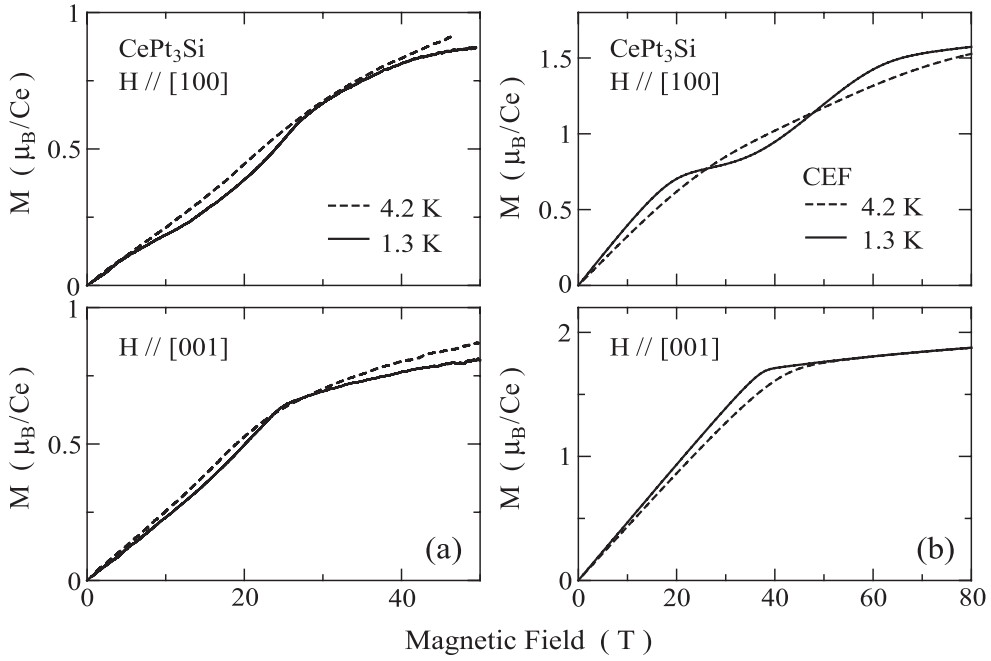

Figure 3. Magnetization curves for the field along [100] and [001] in $CePt_3Si$. The left panel (a) shows the experimental results at 1.3 (solid curves) and 4.2 K (dashed curves) and the light panel (b) represents the corresponding theoretical curves based on the CEF model.

Table 1. CEF parameters, energy level schemes and corresponding wavefunctions for $CePt_3Si$.

CEF parameters						
	B_2^0 (K)	B_4^0 (K)	B_4^4 (K)	λ (emu mol^{-1})$^{-1}$		
	−1.2	−0.79	3.5	−37		
Energy levels and wavefunctions						
E (K)	$\|-5/2\rangle$	$\|-3/2\rangle$	$\|-1/2\rangle$	$\|+1/2\rangle$	$\|+3/2\rangle$	$\|+5/2\rangle$
280	−0.37	0	0	0	−0.93	0
280	0	−0.93	0	0	0	−0.37
12	0	0	1	0	0	0
12	0	0	0	1	0	0
0	0.93	0	0	0	−0.37	0
0	0	−0.37	0	0	0	0.93

around 5 K. The temperature dependence of α also shows positive and negative peaks at the same temperature with a long tail towards higher temperatures along [110] and [001], respectively. These features are reminiscent of the Schottky excitations arising from a CEF splitting of the Hund's-rule ground-state multiplet [9, 10]. Solid curves in figure 4 show the result of CEF calculations, which are described later.

Here it is noted that the initial slope of the pressure dependence of the ordering temperature can be estimated from the Ehrenfest relation by using the values of α and C/T as $\mathrm{d}T_N/\mathrm{d}p = V_m\Delta\alpha_V/\Delta(C/T)$, where V_m is the molar volume, $\Delta\alpha_V$ and $\Delta(C/T)$ are the changes in the volume thermal expansion coefficient and the specific heat divided by

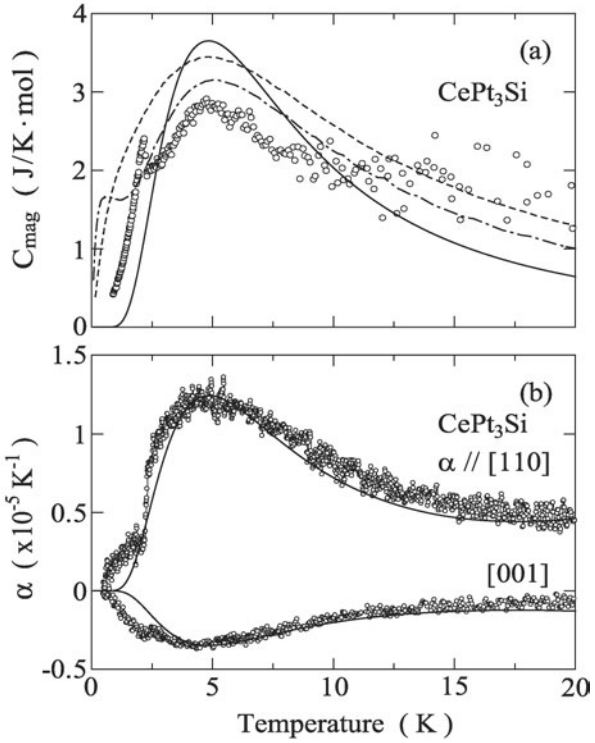

Figure 4. The temperature dependence of the magnetic specific heat $C_{\rm mag}$ (a) and thermal expansion coefficient along [110] and [001] (b) of $CePt_3Si$. Solid curves are due to the CEF model, and other lines in (a) are explained in the text.

temperature at $T_{\rm N}$. By using the experimental values of $V_{\rm m} = 5.432 \times 10^{-5}$ m^3 mol^{-1}, $\Delta\alpha_{\rm V} = (-0.4 \pm 0.1) \times 10^{-5}$ K^{-1} and $\Delta(C/T) = (0.3 \pm 0.1)$ J K^{-2} mol^{-1}, we obtain $\mathrm{d}T_{\rm N}/\mathrm{d}p = (-0.7 \pm 0.2)$ K GPa^{-1}. The minus sign in $\mathrm{d}T_{\rm N}/\mathrm{d}p$ means a suppression of $T_{\rm N}$ under pressure, which is consistent with the hydrostatic pressure experiment [11].

We will analyse the observed χ, M, $C_{\rm mag}$ and α on the basis of the CEF model, because the CEF excitations were observed in the recent neutron scattering experiment [2]. The CEF Hamiltonian for Ce^{3+} ($J = 5/2$) with C_{4v} point symmetry can be expressed as

$$\mathcal{H}_{\rm CEF} = B_2^0 O_2^0 + B_4^0 O_4^0 + B_4^4 O_4^4, \tag{1}$$

where B_ℓ^m and O_ℓ^m are the CEF parameters and the Stevens operators, respectively [12, 13]. Due to the CEF effect, the sixfold-degenerate 4f levels are split into three doublets with excitation energies Δ_1 and Δ_2 from the ground to the first and second excited states, respectively. The CEF parameters were estimated so as to reproduce the two excitation energies $\Delta_1 = 1$ meV and $\Delta_2 = 24$ meV observed in the inelastic neutron scattering experiment as well as the temperature dependence of the inverse magnetic susceptibility. Precise expressions for χ, M, $C_{\rm mag}$ and α based on the CEF model are used in analogy to the cerium compound $CeAgSb_2$ [10].

The solid lines in figures 2 and 4, and the solid and dashed curves in figure 3(b) show the curves calculated by using the CEF parameters listed in table 1. Here, λ in table 1 means the molecular field contribution, which was used in the susceptibility and magnetization calculations. The magnetic susceptibility above 50 K is well explained by the present CEF model, as shown in figure 2. The deviations of the fitting curves from the experimental

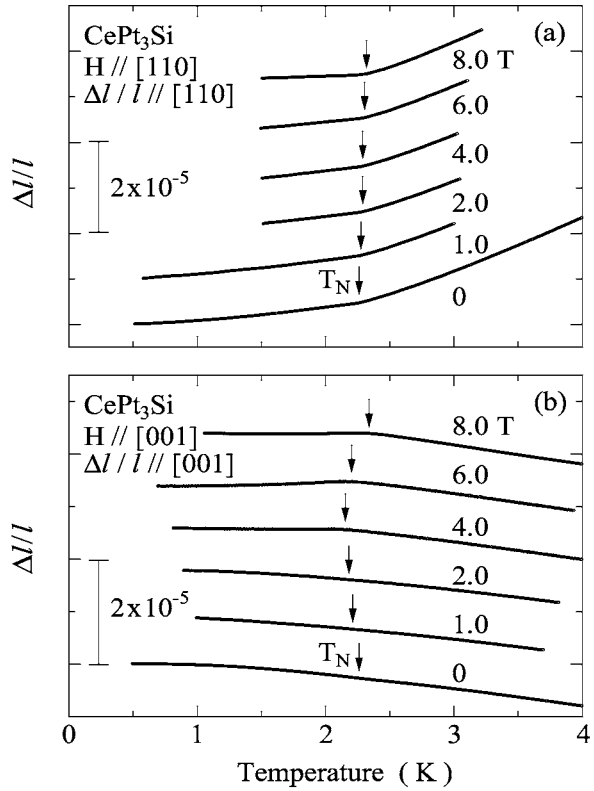

Figure 5. The temperature dependence of the longitudinal thermal expansion for $H \parallel [110]$ (a) and [001] (b) of $CePt_3Si$ in several magnetic fields.

data below 50 K might be due to a substantial Kondo screening at low temperatures, which is closely related to a small ordered moment of 0.16 μ_B [2] and a reduced magnetic entropy at T_N, $0.22R \log 2$ [1]. It is intriguing to compare the calculated CEF magnetization curves with the experimental results, as shown in figure 3. Although the scales for the vertical and horizontal axes are different for the experimental results (a) and the calculations (b), qualitative features in the experimental results can be reproduced by the present CEF curves. The level crossing effect is thus observed even in the antiferromagnetic state, although the metamagnetic-like transition field is modified by the exchange interaction. Such an example was also reported for an antiferromagnet $ErCu_2$ [14]. As mentioned above, the ordered moment of 0.16 μ_B/Ce lies ferromagnetically in the c-plane. This magnitude of the ordered moment is about one fourth as large as the $g_J J_x$(or $g_J J_y$) $= 0.65$ for the ground state in the present CEF scheme. Therefore, the quantitative discrepancy between the experimental and calculated magnetization curves might be due to a moment reduction by the Kondo effect. In order to analyse χ and M in a more realistic way, the magnetic field dependence of the Kondo effect should be considered in the CEF calculation.

The calculated CEF magnetic specific heat and thermal expansion coefficient are shown by solid curves in figure 4 which exhibit a broad peak around 5 K. This can be qualitatively explained as the Schottky peak. However, the peak height in C_{mag} cannot be reproduced by the present simple CEF model, whereas for α, the peak height was treated as a fitting parameter. We calculated the magnetic specific heat following the theory due to Desgranges

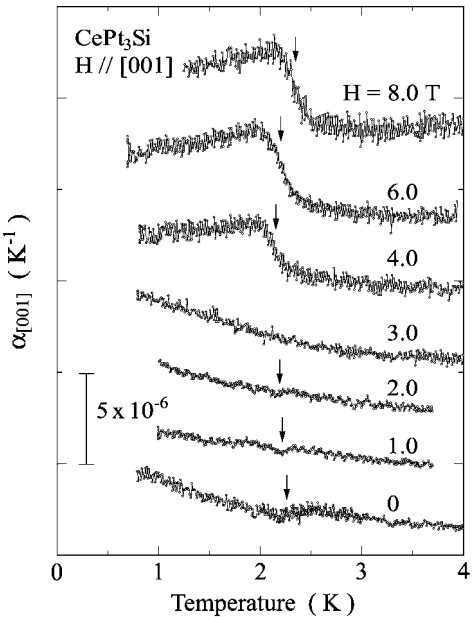

Figure 6. The temperature dependence of the thermal expansion coefficient along [001] in magnetic fields along [001].

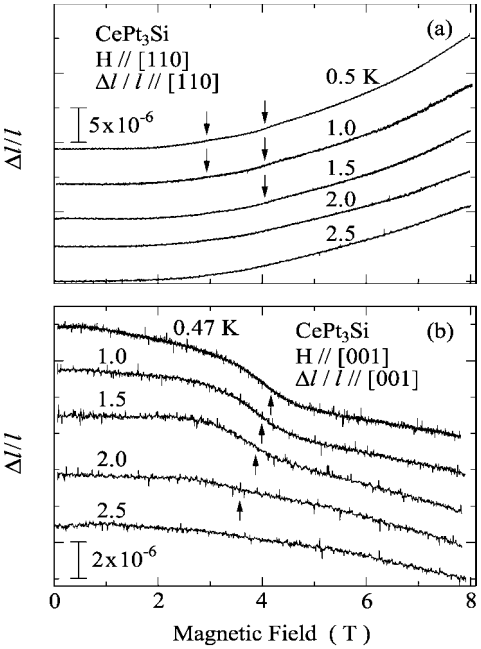

Figure 7. Longitudinal magnetostriction curves for $H \parallel [110]$ (a) and [001] (b) in $CePt_3Si$.

and Rasul which is based on the exact solution of the Coqblin–Schrieffer model including the CEF effect [15, 16]. Dashed and dashed–dotted curves in figure 4(a) are the results for $\Delta_1/T_K = 1$ and 2, respectively, where T_K ($\sim$10 K) is the Kondo temperature. These results provide a better comparison with the experimental data than the pure CEF model. This is due to the fact that the Kondo temperature is comparable to the 4f level splitting energy $\Delta_1 = 12$ K between the ground state and the first excited state.

Finally we constructed the H–T phase diagram for $H \parallel [110]$ and [001] by measuring the thermal expansion under magnetic fields and the magnetostriction. Figures 5(a) and (b) show the longitudinal thermal expansions for $H \parallel [110]$ and [001], respectively. The thermal expansion for $H \parallel [110]$ exhibits a clear kink at the ordering temperature T_N, which is almost unchanged in magnetic fields up to 8 T, as shown in figure 5(a). On the other hand, as shown in figure 5(b), the magnetic field effect on the thermal expansion along [001] is not so simple: the thermal expansion at 0 T increases with decreasing temperature below 4 K, showing a small anomaly at T_N, while above 3 T it decreases slightly below T_N. Correspondingly, T_N shifts to higher temperatures in magnetic fields above 4 T. Since the anomaly in the temperature dependence of the thermal expansion is very weak for $H \parallel [001]$, we determined the ordering temperature T_N at which the thermal expansion coefficient $\alpha_{[001]}$ shows an anomaly, as shown in figure 6.

Figure 7 shows the longitudinal magnetostriction curves for $H \parallel [110]$ (a) and [001] (b) at several temperatures below 2.5 K. For $H \parallel [110]$, the magnetostriction at 2.5 K, which is above T_N, shows a smooth increase up to 8 T. Below T_N, small anomalies were observed around 3 and 4 T, where the magnetostriction exhibits slight changes in slope. It is, however, uncertain whether these anomalies correspond to the phase transition or not. In contrast to the [110] direction, the magnetostriction for $H \parallel [001]$ exhibits a distinct anomaly at about 4 T below T_N, as shown in figure 7(b).

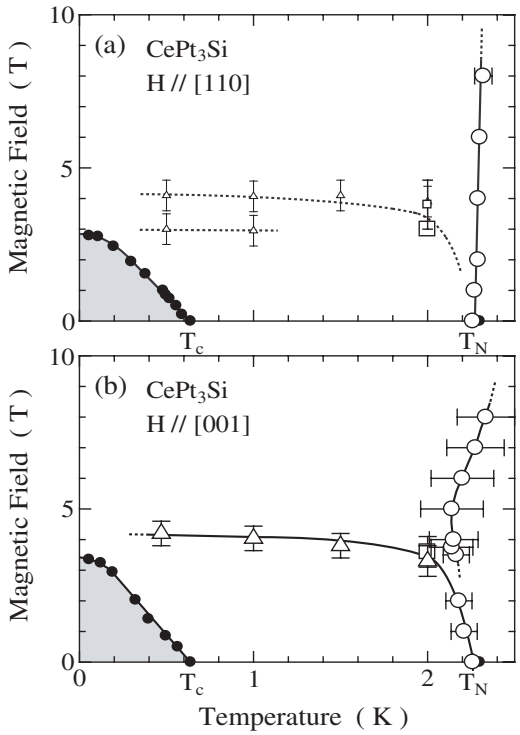

Figure 8. The H–T phase diagram for $H \parallel [110]$ (a) and [001] (b) in $CePt_3Si$. Open circles: the thermal expansion anomaly under fields (figures 5(a) and (b)). Open triangles: magnetostriction anomalies (figures 6(a) and (b)). Open squares: the magnetization anomaly (not shown). Closed circles: the electrical resistivity in magnetic fields (not shown).

From these results, together with the experimental results on the resistivity under magnetic fields and magnetization, we constructed the H–T phase diagram for $H \parallel [110]$ and [001], as shown in figures 8(a) and (b), respectively. The anomalies for $H \parallel [110]$ below T_N are ambiguous, but we nevertheless represented them by small triangles. The superconducting phase is shown by closed circles, which were obtained from the resistivity measurement under magnetic fields [11]. Here the data for $H \parallel [100]$ in the resistivity measurement are shown in figure 8(a), because there is no anisotropy of H_{c2} in the (001) plane.

The H–T phase diagrams are found to be very similar for the two directions, although the anomalies around 4 T for $H \parallel [110]$ below 2 K are not clear at present. A characteristic feature of these phase diagrams is that the antiferromagnetic ordering temperature T_N is almost unchanged up to 8 T for $H \parallel [110]$ and even slightly increases above 4 T for $H \parallel [001]$. This means that the superconducting phase exists deep inside the antiferromagnetic phase with the small ordered moment. The anisotropy for the superconducting phase is also small, namely $H_{c2}(0) = 2.8$ T for $H \parallel [110]$, [001] and $H_{c2}(0) = 3.4$ T for $H \parallel [001]$.

In summary, we grew a single crystal of $CePt_3Si$ and studied its magnetic and thermal properties by measuring the electrical resistivity, specific heat, magnetic susceptibility, high-field magnetization, thermal expansion and magnetostriction. It was found that the simple CEF analyses can qualitatively explain the overall experimental data. Even in the antiferromagnetic state, the CEF model is applicable to the characteristic magnetization curve, indicating the existence of localized magnetic moments, although the ordered moment is

reduced considerably due to the Kondo effect. The superconducting phase exists in this antiferromagnetic phase.

We would like to thank Professor E Bauer for a helpful discussion and Professor S K Dhar for a critical reading of this manuscript. This work was supported by a Grant-in-Aid for Creative Scientific Research (15GS0123) and Scientific Research on Priority Areas from the Ministry of Education, Culture, Sports Science and Technology. One of the authors (TT) is very grateful to the REIMEI Research Resources of Japan Atomic Research Institute for financial support.

References

[1] Bauer E, Hilscher G, Michor H, Paul Ch, Scheidt E W, Gribanov A, Seropegin Yu, Noël H, Sigrist M and Rogl P 2004 *Phys. Rev. Lett.* **92** 027003
[2] Metoki N, Kaneko K, Matsuda T D, Galatanu A, Takeuchi T, Hashimoto S, Ueda T, Settai R, Ōnuki Y and Bernhoeft N 2004 *J. Phys.: Condens. Matter* **16** L207
[3] Steglich F, Aarts J, Bredl C D, Lieke W, Meschede D, Franz W and Schäfer H 1979 *Phys. Rev. Lett.* **43** 1892
[4] Petrovic C, Pagliuso P G, Hundley M F, Movshovich R, Sarrao J L, Thompson J D, Fisk Z and Monthoux P 2001 *J. Phys.: Condens. Matter* **13** L337
[5] Geibel C, Schank C, Thies S, Kitazawa H, Bredl C D, Böhm A, Rau M, Grauel A, Caspary R, Helfrich R, Ahlheim U, Weber G and Steglich F 1991 *Z. Phys.* B **84** 1
[6] Lacerda A, de Visser A, Haen P, Lejay P and Flouquet J 1989 *Phys. Rev.* B **40** 8759
[7] Frings F H, Franse J J M, de Boer F R and Menovsky A 1985 *J. Magn. Magn. Mater.* **31–34** 240
[8] Ōnuki Y, Haga Y, Yamamoto E, Inada Y, Settai R, Yamagami H and Harima H 2003 *J. Phys.: Condens. Matter* **15** S1903
[9] Takeuchi T, Inoue T, Sugiyama K, Aoki D, Tokiwa Y, Haga Y, Kindo K and Ōnuki Y 2001 *J. Phys. Soc. Japan* **70** 877
[10] Takeuchi T, Thamizhavel A, Okubo T, Yamada M, Nakamura N, Yamamoto T, Inada Y, Galatanu A, Yamamoto E, Kindo K, Ebihara T and Ōnuki Y 2003 *Phys. Rev.* B **67** 064403
[11] Yasuda T, Shishido H, Hashimoto S, Takeuchi T, Settai R and Ōnuki Y 2004 at press
[12] Stevens K W H 1952 *Proc. Phys. Soc.* A **65** 209
[13] Hutchings M T 1965 *Solid State Physics: Advances in Research and Applications* vol 16, ed F Seitz and B Turnbull (New York: Academic) p 227
[14] Sugiyama K, Yamamoto T, Nakamura N, Thamizhavel A, Yoshii S, Kindo K, Luong N H and Ōnuki Y 2003 *Physica* B **327** 423
[15] Desgranges H-U and Rasul J W 1985 *Phys. Rev.* B **32** 6100
[16] Desgranges H-U and Rasul J W 1987 *Phys. Rev.* B **36** 328